Materials Horizons

ROYAL SOCIETY OF CHEMISTRY

COMMUNICATION

View Article Online
View Journal | View Issue

Cite this: *Mater. Horiz.*, 2023, **10**, 4251

Received 2nd June 2023,
Accepted 26th July 2023

DOI: 10.1039/d3mh00839h

rsc.li/materials-horizons

Inclination of polarized illumination increases symmetry of structures grown *via* inorganic phototropism†

Madeline C. Meier, [a] Nathan S. Lewis *[ab] and Azhar I. Carim *[ab]

Inclination of unpatterned, linearly polarized illumination in the plane of the electric field oscillation effected increased directional feature alignment and decreased off-axis order in Se–Te deposits generated by inorganic phototropic growth relative to that produced using normal incidence. Optically based growth simulations reproduced the experimental results indicating a photonic basis for the morphology change. Modeling of the light scattering at the growth interface revealed that illumination inclination enhances scattering that localizes the optical field along the polarization plane and suppresses cooperativity in defect-driven scattering. Thus, the symmetry of the deposited structures increased as the asymmetry of the illumination increased, as measured by the inclination of the illumination incidence away from the surface normal.

New concepts

Inorganic phototropic growth, in which electrochemical semiconductor deposition is directed towards light in a manner resembling the natural phototropic growth of plants, produces ordered mesostructured deposits in response to low intensity, spatially uniform far-field illumination, despite a lack of optical anisotropy in the growth solution or on the electrode substrate. The mesoscale deposit structure is determined by the properties of the stimulating illumination, including the polarization and the wavelength. Growth using illumination inclined in the polarization plane increased the nanoscale symmetry of the resulting mesostructures as compared to growth using normally incident illumination. The uniformity of such structures can thus be manipulated by use of various steady-state optical inputs, without lithographic templating or use of chemical structure-directing agents. The observed morphological control expands the capability of inorganic phototropic growth to generate custom nanoarchitectures in a programmable manner based only on the properties of the incident light during growth.

[a] *Division of Chemistry and Chemical Engineering, California Institute of Technology, Pasadena, CA 91125, USA. E-mail: nslewis@caltech.edu, aic@caltech.edu*

[b] *Beckman Institute, California Institute of Technology, Pasadena, CA 91125, USA*

† Electronic supplementary information (ESI) available. See DOI: https://doi.org/10.1039/d3mh00839h

Nathan S. Lewis

Congratulations on the fantastic first ten years, Materials Horizons! It has been remarkable to witness how your journal has consistently elevated its profile and prestige through a commitment to highlighting the most cutting-edge research and innovation. We are thus excited to report here an unexpected result that contradicted intuition, sparked our scientific curiosity, and added a new dimension to the subject. Here's to another decade of continuous growth and impact!

Photoelectrochemical deposition of semiconductor materials by inorganic phototropic growth spontaneously generates ordered mesostructures with nanoscale features despite the lack of a photomask or any physical or chemical templating agents.[1–3] Deposition of material is directed towards local maxima in the interfacial optical field, similar to the plasmon-mediated photochemical growth of metallic nanoparticles.[4,5] Inorganic phototropic growth is analogous to natural phototropism in which plants extend responsively toward light and develop morphologies determined by the illumination available in the environment, *e.g.*, the curved growth of house plants towards a window and the tall unbranched growth of understory trees towards a forest canopy.[6–8] As with natural phototropism, the illumination inputs define the structures generated by inorganic phototropic growth.[9–12] Low-intensity, linearly polarized, incoherent illumination generates ordered, anisotropic lamellar structures with a pitch that is proportional to the source wavelength and a morphological orientation that is set by the optical polarization vector.[9,10] Herein, we report that asymmetric inclination of the illumination

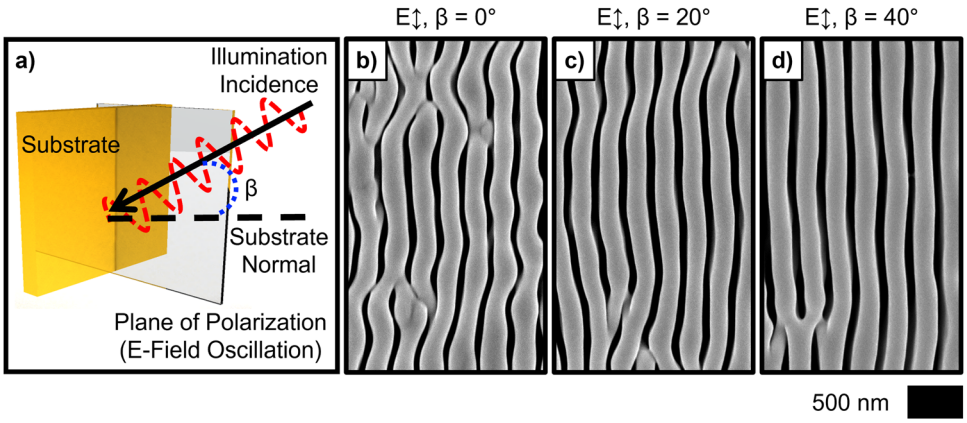

Fig. 1 (a) Schematic illustration of electrode substrate illumination with linearly polarized light inclined in the plane of the polarization. (b)–(d) Representative SEMs of deposits generated with vertically polarized (E ↕) λ_{avg} = 626 nm illumination with the indicated inclination (β) from the substrate normal in the plane of the polarization.

input in the plane of the polarization increases deposit structural symmetry by improving uniaxial feature alignment and reducing off-axis order. Fourier analysis was used to assess morphological order and optical simulations were performed to examine the mechanistic basis for the variation in uniformity.

Fig. 1a presents a schematic illustrating the illumination of an electrode substrate with linearly polarized light inclined from the substrate normal in the plane of the polarization by an angle β. Fig. 1b presents a scanning-electron micrograph (SEM) of a Se–Te deposit generated *via* inorganic phototropic growth using vertically polarized λ_{avg} = 626 nm illumination from a light-emitting diode (LED) source directed along the substrate normal ($\beta = 0^\circ$). Even though the illumination was unpatterned, the deposit exhibited an ordered and anisotropic lamellar morphology, with substantial horizontal periodicity and a net orientation of the lamellar long axes towards the vertical. Along the length, individual lamellar features were sinuous and exhibited alternating deviations from vertical alignment as well as fluctuations in width. These irregularities generated some off-axis order, away from the horizontal. Dislocation defects were also observed, in which two adjacent features exhibited segments that were oriented off-axis and converged to a single feature. Fig. 1c and d present SEMs of deposits generated under the same conditions as in Fig. 1b but with the illumination inclined with $\beta = 20^\circ$ and 40°, respectively. For $\beta = 20^\circ$, the individual features exhibited a lower frequency of deviations from the vertical than was observed for normal incidence ($\beta = 0^\circ$, Fig. 1b), but off-axis feature segments and dislocation defects were still frequently observed. The feature width was more consistent along the length than with illumination along the surface normal. For $\beta = 40^\circ$, the frequency at which off-axis features were observed was substantially reduced relative to the $\beta = 0^\circ$ and 20° cases, and the translational symmetry of the structure in both the vertical and horizontal directions was enhanced. Thus, inclination in the plane of the polarization of the illumination input improved the uniformity of films produced by the inorganic phototropic growth process.

Fourier analysis was utilized to assess the order of the deposits generated *via* inorganic phototropic growth using either normally incident or inclined illumination. Fig. 2a–c presents two-dimensional Fourier transforms (2D FT) generated from SEMs of deposits produced using $\beta = 0^\circ$, 20° and 40°, respectively. The intensity in a FT is indicative of the magnitude of a spatially periodic morphology component in the deposit

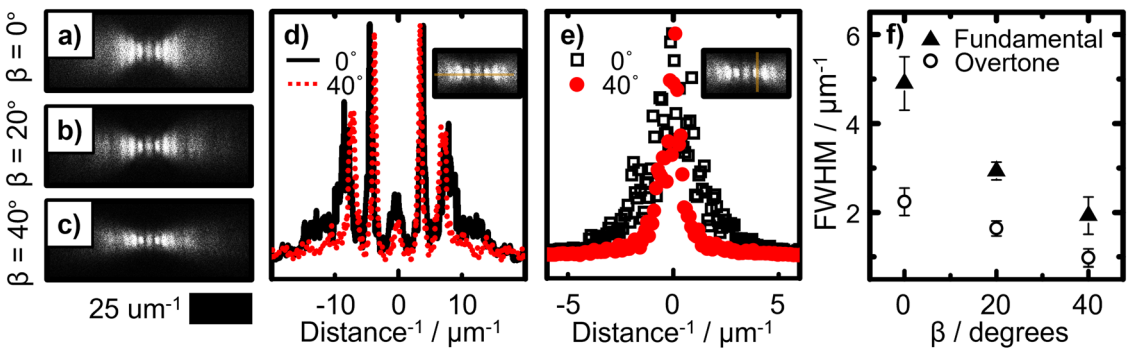

Fig. 2 (a)–(c) 2D FTs generated from SEM data of the deposits depicted in Fig. 1(b)–(d) respectively. (d) Fourier spectra representing the intensity along the horizontal centerlines of the 2D FTs depicted in (a) and (c). (e) Fourier spectra representing the intensity along the vertical centerlines of the positive fundamental modes in the 2D FTs in (a) and (c). (f) FWHM of fit curves of spectral profiles similar to those in (e) for the positive fundamental and first overtone modes in the 2D FTs in (a)–(c) as a function of β.

from which the FT was derived. The displacement distance from the center of the FT is the spatial frequency, and the direction of the displacement is the direction of the spatial periodicity. For all three values of β, the 2D FTs exhibited a single set of intense bands aligned along the horizontal, consistent with the anisotropy and horizontal periodicity in the deposit morphologies (Fig. 1b–d). Fig. 2d presents Fourier spectra representing the intensity profiles along the horizontal centerlines of the 2D FTs for $\beta = 0^\circ$ and 40° (Fig. 2a and c). The spectra were mutually similar qualitatively, and both revealed a single family of harmonics, indicative of morphologies having a single, narrow range, of pitch values.[9] The substantial overtone intensity is consistent with the sharp contrast in the SEM data (Fig. 1b–d), and thus confirms the presence of substantial structural anisotropy. The structure topologies could not be fully represented by a single sinusoidal function, but instead were more fully described by a function similar to a square-wave that required the higher-frequency overtone intensity to approximate. The harmonic bandwidths for $\beta = 40^\circ$ were qualitatively narrower than for $\beta = 0^\circ$, indicating a more consistent feature pitch across the interface. The Fourier spectrum for $\beta = 40^\circ$ also showed less intensity at zero frequency, as well as lower baseline intensity relative to the spectrum for $\beta = 0^\circ$, indicating a reduction in aperiodic morphological components as well as more well-defined order in deposits produced using inclined illumination.

Notably, the intensity bands in the 2D FT derived from the SEM data for $\beta = 0^\circ$ (Fig. 2a) showed clearly observable height in the vertical direction (perpendicular to the direction of the morphological periodicity), with the band height increasing with each successive harmonic. The presence of intensity off the horizontal axis is consistent with the observed off-axis feature alignments (Fig. 1b). The vertical height of the bands, as well as the degree of height increase in the successive overtones, decreased for $\beta = 20^\circ$ (Fig. 2b), and further decreased for $\beta = 40^\circ$ (Fig. 2c), consistent with the improved feature alignment observed in the morphologies as the illumination inclination increased. Fig. 2e presents Fourier spectra representing the intensity profiles across the vertical centerlines of the positive fundamental modes of the 2D FTs for $\beta = 0$ and 40°. In these profiles, the positive and negative modes are degenerate due to the intrinsic symmetry of the 2D FT, so the choice of mode for analysis was arbitrary. Fig. S2 (ESI†) presents the same profiles as in Fig. 2e along with associated fit curves. Fig. 4f presents the full width at half maximum (FWHM) derived from fit curves of the Fourier spectra as a function of β for both the fundamental and first overtone modes of each 2D FT. The FWHM of both modes was approximately 60% lower for $\beta = 40^\circ$ than for $\beta = 0^\circ$, with intermediate values observed for $\beta = 20^\circ$. This analysis confirms that the apparent improvement in morphological uniformity produced by use of inclined illumination is primarily due to a reduction in off-axis morphological order. The large absolute decrease in the overtone FWHM as β increased, more than twofold larger than the decrease in the fundamental FWHM, is indicative of a substantial decrease in the off-axis topological contrast.

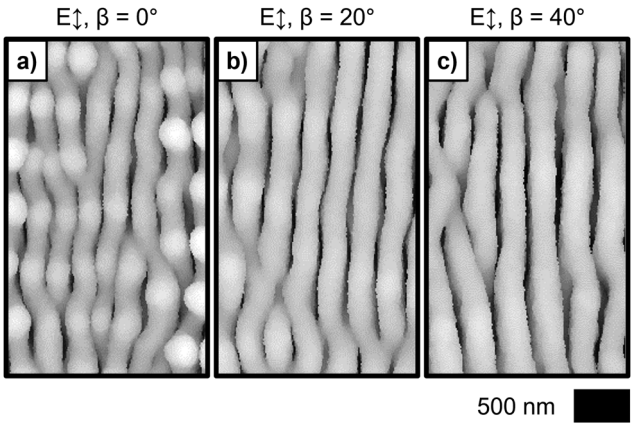

Fig. 3 Simulated deposit morphologies generated *via* growth modeling with vertically polarized (E ↕) λ_{avg} = 626 nm illumination with the indicated inclination (β) from the substrate normal in the plane of the polarization.

A series of simulations was performed to elucidate the mechanism by which inclination of the illumination input improved the feature alignment and reduced off-axis order in the structures formed by inorganic phototropic growth. Growth was simulated using an optically based, two-step iterative model. First, an electromagnetic simulation was used to calculate the local light absorption profile. Next, a Monte Carlo simulation was performed to simulate growth in which the absorption profile was used to define the probability of local material addition, and the process was then iterated. Empirical inputs to the model were limited to estimates of the index of refraction of the deposition solution and the complex refractive index of the deposit. Fig. 3a–c presents simulated morphologies generated *via* growth modeling using vertically polarized λ_{avg} = 626 nm illumination inclined at $\beta = 0^\circ$, 20° and 40°, respectively. In all cases, the simulated morphologies qualitatively reproduced the experimental results (Fig. 1b–d). For $\beta = 0^\circ$, the lamellar features were sinuous and exhibited variable width along the long axes and dislocation defects were also observed (Fig. 2a). The alignment variance of local feature segments decreased, and the feature width along a single lamellar feature became more consistent, as β increased from $\beta = 0^\circ$ to $\beta = 20^\circ$ (Fig. 2b). For $\beta = 40^\circ$ (Fig. 2c), the linearity increased further along the length of the individual features relative to growth using $\beta = 0^\circ$ and 20°. The agreement between the results of the model, generated by considering only optical interactions, and the experimental data are consistent with a photonic basis for the symmetry improvement observed for the use of inclined illumination, irrespective of any chemical or crystallographic effects.[13,14]

Structure generation *via* inorganic phototropic growth is a product of inherent asymmetries in the interfacial light-matter interactions that shape the local optical field profile, which in turn directs the local rates of photoelectrochemical deposition. At the onset of deposition, the substrate is isotropic, but initial electrochemical growth driven by an applied external bias reduces the symmetry of the interface by generating surface texture that scatters the incident illumination. The linear

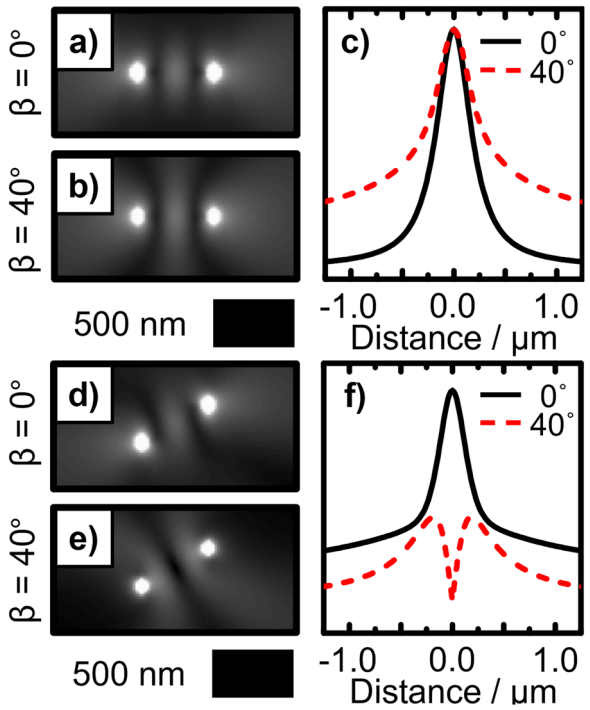

Fig. 4 (a) Simulation of the normalized time-average electric field magnitude from two coherent dipole sources emitting radiation with a free space wavelength of λ = 626 nm in a medium of refractive index n = 1.33. The dipole oscillation axis was along the vertical and the dipoles were separated by one wavelength along the horizontal. (b) Same as (a) but with the dipole oscillation axis inclined 40° into the simulation plane. (c) Line profiles of the field magnitude from the simulations in (a) and (b) along the axis perpendicular to the separation axis and through the separation midpoint. (d) and (e) Same as (a) and (b), respectively, but with the dipole sources separated along a diagonal axis. (f) Similar line profiles as in (c) but corresponding to the simulations in (d) and (e).

polarization results in directional scattering and concerted behavior across the interface generates a non-uniform field profile that promotes anisotropic deposition.[10] Continued ordered, anisotropic growth that yields well-defined lamellar features consequently results from an emergent nanophotonic positive feedback loop in which individual features scatter light directionally towards neighboring features, generating synergistic absorption.[15]

Computer modeling was used to examine the effect of illumination inclination on the local field profile that results from the scattering processes at the growth interface. Point dipole sources were used to represent scattering sites. Fig. 4a presents a simulation of the normalized time-average electric field magnitude from two coherent dipole sources emitting radiation with a free space wavelength of λ = 626 nm in a medium having a refractive index of n = 1.33. The dipole oscillation axis was along the vertical, and the dipoles were separated by one wavelength along the horizontal. Fig. 4b presents a similar simulation but with the dipole oscillation axis inclined 40° into the simulation plane. In both cases, a vertically aligned band of intensity was observed midway between the dipoles, consistent with the generation of an anisotropic lamellar feature at a location one characteristic feature pitch away from the dipole sources. However, the height of the band was greater in the case with the dipole oscillation axes inclined (Fig. 4b) relative to that with the axes in-plane (Fig. 4a). Fig. 4c presents profiles of the field magnitude along the vertical centerline obtained from the simulations in Fig. 4a and b. The field magnitudes were mutually similar at the center, and for the inclined case the field magnitude was increased away from center relative to the in-plane case. Inclination of the illumination can therefore increase the anisotropy of the scattered field profile in the plane of the input polarization, promoting the growth of longer vertically aligned feature segments in a manner consistent with the experimental observations (Fig. 1b–d).

Additional simulations were performed to specifically assess the effect of illumination inclination on the generation of off-axis order. Fig. 4d presents a simulation similar to Fig. 4a but with the dipoles separated along a diagonal axis. An intensity band was observed with an alignment away from the vertical axis. Despite the vertical polarization, off-vertical anisotropy in the local field magnitude can be generated, and thus initial defects in the structure may be reinforced to produce ordered off-axis growth in a manner deleterious to the overall uniformity of the structure. This growth process is consistent with the observation of a "history effect" in inorganic phototropic growth in which a preexisting structure affects the morphological habit of subsequently deposited films.[16] The modeling results are thus also consistent with the observed increase in the fidelity of deposition on substrates that were initially lithographically templated with metal lines having a characteristic feature pitch in accord with the pitch observed when growth was performed on an untemplated substrate.[17]

Fig. 4e presents a simulation with two dipole sources separated diagonally, similar to that in Fig. 4d, but with the oscillation axes inclined 40° into the simulation plane. For this inclined case, no intensity band was observed at the midpoint of the separation axis. Fig. 4f presents field magnitude profiles from the simulations in Fig. 4d and e, along a line perpendicular to the dipole separation axis and through the simulation midpoint. The profile corresponding to the in-plane case was qualitatively similar to the profiles for the simulations having dipoles separated along the horizontal (Fig. 4c). However, the profile corresponding the inclined case exhibited a minimum at the center, and the magnitude at all positions in the profile was lower than for the in-plane case. This behavior indicates that inclination of the illumination decreases the scattering cooperativity that promotes ordered off-axis growth, and thus enhances the preferential generation of anisotropic features that have a periodicity perpendicular to the plane of the input polarization. This finding is consistent with the increased symmetry observed experimentally in the deposits (Fig. 1b–d) as well as the reduction in the off-axis intensity in the associated 2D FT data (Fig. 2).

The data collectively demonstrate that, counterintuitively, an increase in the asymmetry of the illumination input

resulting from off-normal inclination increases the symmetry and uniformity of the mesostructures generated by inorganic phototropic growth. Such a change is produced in a straightforward manner without the use of any templating agents, by capitalizing on unique light-matter interactions. Relative to the case of normal incident illumination, inclined illumination improves the alignment of features along the plane of the input polarization and decreases the off-axis order in the deposit. Modeling of the interfacial light scattering during growth indicates that inclination of the illumination incidence can increase the spatial anisotropy of the scattered optical field magnitude in the direction parallel to the input polarization plane, stimulating the generation of longer vertically aligned feature segments. Similar modeling also indicates that inclination of the illumination incidence decreases the scattering cooperativity at defect sites and thus curtails ordered off-axis growth. Fidelity control in this work was thus effected solely by controlling the optical input, which consequently may be useful in the programmable, bottom-up generation of artificial analogs of biological interfaces with useful physical properties that are characterized by ordered features similar to those generated *via* inorganic phototropic growth.[18,19]

Conflicts of interest

The authors declare no conflict of interest.

Acknowledgements

This work was supported by the National Science Foundation, Directorate for Mathematical & Physical Sciences, Division of Materials Research under Award Number DMR 1905963. Research was in part carried out at the Molecular Materials Resource Center in the Beckman Institute of the California Institute of Technology. The authors gratefully acknowledge J. Thompson for insightful discussions, W.-H. Cheng and S. Yalamanchili for assistance with substrate preparation, and R. Gerhart, N. Hart, and B. Markowicz for assistance with photoelectrochemical cell fabrication. MCM acknowledges a Graduate Research Fellowship from the National Science Foundation and the Resnick Institute at Caltech for fellowship support.

References

1 B. Sadtler, S. P. Burgos, N. A. Batara, J. A. Beardslee, H. A. Atwater and N. S. Lewis, *Proc. Natl. Acad. Sci. U. S. A.*, 2013, **110**, 19707–19712.
2 A. I. Carim, K. R. Hamann, N. A. Batara, J. R. Thompson, H. A. Atwater and N. S. Lewis, *J. Am. Chem. Soc.*, 2018, **140**, 6536–6539.
3 K. R. Hamann, A. I. Carim, M. C. Meier, J. R. Thompson, N. A. Batara, I. S. Yermolenko, H. A. Atwater and N. S. Lewis, *J. Mater. Chem. C*, 2020, **8**, 12412–12417.
4 R. Jin, Y. Cao, C. A. Mirkin, K. L. Kelly, G. C. Schatz and J. G. Zheng, *Science*, 2001, **294**, 1901–1903.
5 R. Jin, Y. C. Cao, E. Hao, G. S. Métraux, G. C. Schatz and C. A. Mirkin, *Nature*, 2003, **425**, 487–490.
6 M. C. Meier, W.-H. Cheng, H. A. Atwater, N. S. Lewis and A. I. Carim, *J. Am. Chem. Soc.*, 2019, **141**, 18658–18661.
7 C. W. Whippo and R. P. Hangarter, *Plant Cell*, 2006, **18**, 1110–1119.
8 N. C. Arens and P. S. Baracaldo, *Am. Fern J.*, 2000, **90**, 1–15.
9 A. I. Carim, N. A. Batara, A. Premkumar, H. A. Atwater and N. S. Lewis, *Nano Lett.*, 2015, **15**, 7071–7076.
10 A. I. Carim, N. A. Batara, A. Premkumar, H. A. Atwater and N. S. Lewis, *ACS Nano*, 2016, **10**, 102–111.
11 A. I. Carim, N. A. Batara, A. Premkumar, R. May, H. A. Atwater and N. S. Lewis, *Nano Lett.*, 2016, **16**, 2963–2968.
12 K. R. Hamann, M. C. Meier, N. S. Lewis and A. I. Carim, *JACS Au*, 2022, **2**, 865–874.
13 Z.-L. Xiao, C. Y. Han, W.-K. Kwok, H.-H. Wang, U. Welp, J. Wang and G. W. Crabtree, *J. Am. Chem. Soc.*, 2004, **126**, 2316–2317.
14 M. J. Siegfried and K.-S. Choi, *J. Am. Chem. Soc.*, 2006, **128**, 10356–10357.
15 A. I. Carim, M. C. Meier, K. M. Kennedy, M. H. Richter, K. R. Hamann and N. S. Lewis, *J. Am. Chem. Soc.*, 2021, **143**, 3693–3696.
16 K. R. Hamann, A. I. Carim, M. C. Meier and N. S. Lewis, *J. Am. Chem. Soc.*, 2020, **142**, 19840–19843.
17 E. Simonoff, J. R. Thompson, M. C. Meier, K. M. Kennedy, K. R. Hamann and N. S. Lewis, *J. Phys. Chem. C*, 2021, **125**, 9571–9581.
18 D. Xia, L. M. Johnson and G. P. Lopez, *Adv. Mater.*, 2012, **24**, 1287–1302.
19 S. Kinoshita and S. Yoshioka, *Chem. Phys. Chem.*, 2005, **6**, 1442–1459.